Computers, Materials & Continua CMC, vol.65, no.1, pp.433-443, 2020

Multi-Directional Reconstruction Algorithm for Panoramic Camera

Shi Qiu[1], Bin Li [2, *], Keyang Cheng[3], Xiao Zhang[2], Guifang Duan[4] and Feng Li[5]

Abstract: A panorama can reflect the surrounding scenery because it is an image with a wide angle of view. It can be applied in virtual reality, smart homes and other fields as well. A multi-directional reconstruction algorithm for panoramic camera is proposed in this paper according to the imaging principle of dome camera, as the distortion inevitably exists in the captured panorama. First, parameters of a panoramic image are calculated. Then, a weighting operator with location information is introduced to solve the problem of rough edges by taking full advantage of pixels. Six directions of the mapping model are built, which include up, down, left, right, front and back, according to the correspondence between cylinder and spherical coordinates. Finally, multi-directional image reconstruction can be realized. Various experiments are performed in panoramas (1024×1024) with 30 different shooting scenes. Results show that the azimuth image can be reconstructed quickly and accurately. The fuzzy edge can be alleviated effectively. The rate of pixel utilization can reach 84%, and it is 33% higher than the direct mapping algorithm. Large scale distortion is also further studied.

Keywords: Panorama, multi-angle, reconstruction, weighting operator.

1 Introduction

The panoramic technique has been extensively applied in many industries such as in meteorology, photography, movie and television, medical science, security monitoring, defense and military affairs and other fields [Pan, Qin, Chen et al. (2019)]. It also has become one research hotspot in computer graphic and visual science [Sandnes and Huang (2016); Cheng, Xu, Tao et al. (2018); Qiu, Luo, Yang et al. (2019)].

A large number of images with overlapping regions can be shot by a single horizontal

[1] Key Laboratory of Spectral Imaging Technology CAS, Xi'an Institute of Optics and Precision Mechanics, Chinese Academy of Sciences, Xi'an, 710119, China.

[2] School of Information Science and Technology, Northwest University, Xi'an, 710127, China.

[3] School of Computer Science and Communication Engineering, Jiangsu University, Zhenjiang, 212013, China.

[4] State Key Laboratory of CAD & CG, Zhejiang University, Hangzhou, 310058, China.

[5] Institute of Education, University College London, London, UK.

[*] Corresponding Author: Bin Li. Email: lib@nwu.edu.cn.

Received: 16 January 2020; Accepted: 19 May 2020.

rotating camera and then they can be stitched by post calculation. Yuan et al. [Yuan, Pan, Sheu et al. (2013)] removed the artifacts of images by constructing a feature fusion model. Liu et al. [Liu, Zhao, Li et al. (2014); Zeng, Zhang, Zhang et al. (2014)] proposed the feature dynamic mosaic images based on SIFT. Shaikh et al. [Shaikh and Patankar (2015)] used the optimized MKL for SPM to classify images. Zhang et al. [Zhang, Liang, Yang et al. (2018)] applied a robust forgery detection algorithm into object removal to blend multiple features for image splicing. Alomran et al. [Alomran and Chai (2016)] proposed a feature algorithm based on global images. Cai et al. [Cai, Wang and Liang (2016)] improved the SURF and proposed a fast global image mosaic algorithm. Tehrani et al. [Tehrani, Garratt and Anavatti (2016)] built a probability statistical model to achieve low-altitude image stitching. Pham et al. [Pham, Lee, Kwon et al. (2019)] proposed an image splicing detection algorithm based on Markov features. They shot with multiple cameras in different angles firstly, and then stitched the pictures.

Multiple images can be shot with a general lens, and their overlapping regions can be stitched. Mühlhausen et al. [Mühlhausen, Moritz and Marcus (2020)] proposed a multiview panorama alignment and optical flow refinement. Sharpless et al. [Sharpless, Postle and German (2010)] applied the wide-angle painting geometric composition theory successfully, which was proposed by the famous painter. Their algorithm combined the perspective projection with the spherical plane projection, and overcame the tensile deformation of the perspective projection at the edge of the image. The panorama displayed a range within 180°. Wei et al. [Wei, Li, Hu et al (2011); Sacht and Velho (2013)] proposed a fisheye video correction algorithm, which built six constraint equations to reduce the image deformation, and minimized the correction function to realize the control of the deformation. Zhang et al. [Zhang, Liang, Yang et al. (2017)] utilized multi-scale spatial and spectral entropies for image seam carving with low scaling ratio. Zhu et al. [Zhu, Liu, Lai et al. (2016)] used a fisheye wide-angle lens to shoot limited number of frames for correction and splicing in order to form a panoramic image. Ma et al. [Ma, Liu, Zhang et al. (2015); Cheng, Hui, Zhan et al. (2017)] utilized the radiological model to correct the large-angle image distortion. Shi et al. [Shi, Lei and Wan (2019)] proposed the spatial calibration method for master-slave camera based on panoramic image mosaic.

Mirror reflection or an optical equipment can be used to obtain any direction of information (horizontal 360°, vertical nearly 360°), and an imaging to avoid the process of image stitching [Lee, Kim, Kim et al. (2016)]. Although the price is high and is not universal, it has broad research space and is the main direction of future research. We have studied the panoramic camera for rapid reconstructing multi-azimuth images. Thus, it can intuitively observe images from each perspective, especially from the top. This article consists of four sections in total. Section 2 introduces the proposed algorithm, Section 3 performs the experiment and analysis, and Section 4 concludes the article.

2 Multi-directional reconstruction algorithm

Panoramic cylindrical images are shot by dome cameras. These images are distorted in some extent, and the deformation is obvious when the field of view is greater than 90°, as shown in Fig. 1 (beam, ground and so on). Thus, the mapping model is constructed

according to the correspondence between spherical and cylindrical coordinates and the panorama is corrected. Finally, the accurate image of each field of view can be obtained.

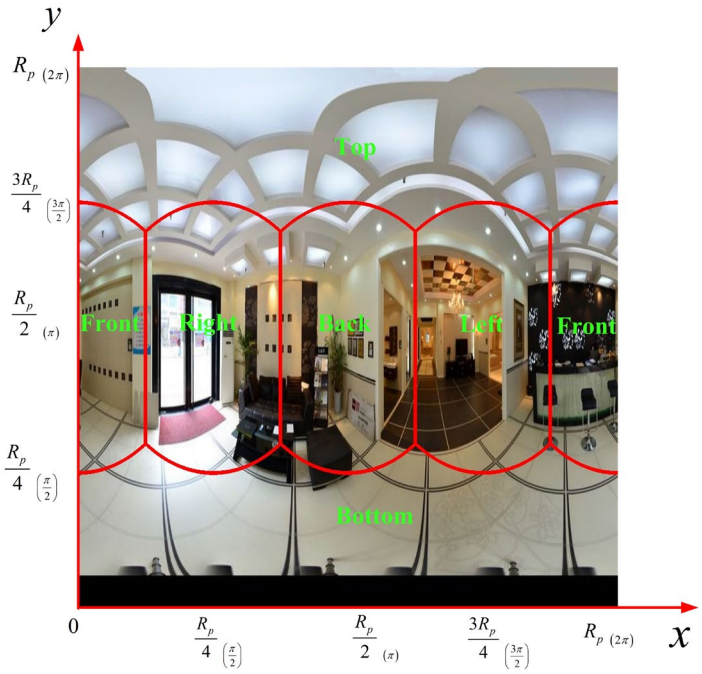

Figure 1: The panoramic image

2.1 Parameter calculation

The horizontal field of view of the dome camera is (0°~360°) and the vertical field of view of the dome camera is (0°~340°). The relationship between the cylindrical image and the spherical image is as follows:

$$R = \frac{R_p}{2 \times \pi} \tag{1}$$

$$\alpha = \frac{2\pi x_p}{R_p} \tag{2}$$

$$\beta = \frac{2\pi y_p}{R_p} \tag{3}$$

where $R_p \times R_p$ is the resolution of the cylindrical image; R is the radius of the spherical image; α is the degree in the horizontal direction; β is the degree in the vertical direction.

The square area with R_v=2R is as the field of view. Six directions include up, down, left, right, front and back. The mapping relationship is shown in Fig. 2.

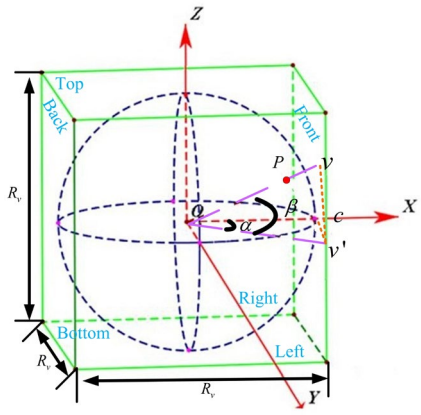

Figure 2: The relations between six angles

2.2 The four image view reconstruction

The front, back, left and right directions are based on the horizontal plane, and the algorithm is illustrated by the front direction, as shown in Fig. 3(a). The point on the front plane is (x_v, y_v). v' is the projection along the Y-axis. The projection plane is shown in Fig. 3(b).

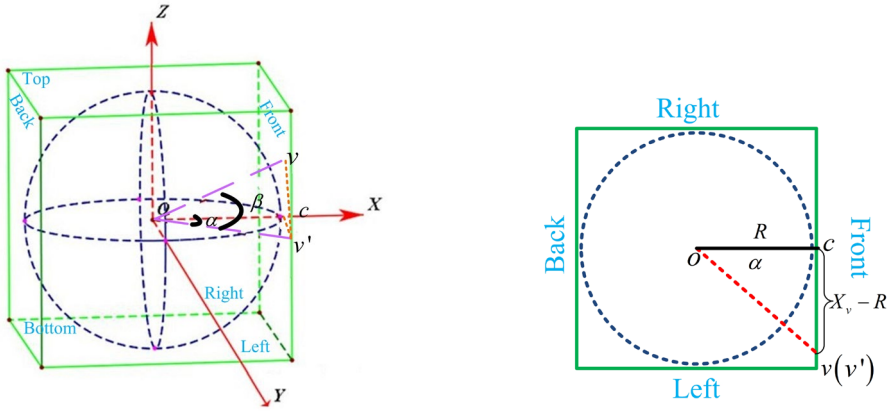

(a) The stereoscopic image (b) The image from X-axis direction projection

Figure 3: The image form horizontal angle

Calculate α and β from the geometry as follows:

$$\alpha = \begin{cases} \arctan\dfrac{x_v - R}{R} + \delta & 0 \le \arctan\dfrac{x_v - R}{R} + \delta \le 2\pi \\ \arctan\dfrac{x_v - R}{R} + \delta\text{-}2\pi & \arctan\dfrac{x_v - R}{R} + \delta > 2\pi \\ \arctan\dfrac{x_v - R}{R} + \delta + 2\pi & \arctan\dfrac{x_v - R}{R} + \delta < 0 \end{cases} \tag{4}$$

$$\beta = \arctan \frac{\left(y_v - R\right)}{\sqrt{\left(x_v - R\right)^2 + R^2}} \tag{5}$$

where δ is the radian in the center of the horizontal direction ($\delta_{\text{Right}} = \frac{\pi}{2}$, $\delta_{\text{Left}} = \frac{3\pi}{2}$, $\delta_{\text{Back}} = \pi$, $\delta_{\text{Front}} = 2\pi$). The coordinate value (x_p, y_p) of the corresponding point is calculated as follows:

$$x_p = \begin{cases} 0 & \alpha < 0 \\ \frac{\alpha}{2\pi} \times R_p & 0 \leqslant \alpha \leqslant 2\pi \\ R_p\text{-}1 & \alpha > 2\pi \end{cases} \tag{6}$$

$$y_p = \left(\frac{1}{2} + \frac{\beta}{\pi}\right) \times R_p \tag{7}$$

The mapping coordinate is constructed. $V_{(x_v, y_v)}$ is the pixel value of point (x_v, y_v) and $F(\ )$ is the mapping function, respectively.

$$V_{(x_v, y_v)} = F\left(x_p, y_p\right) \tag{8}$$

2.3 The image view of bottom and top reconstruction

The bottom and top field of views calculated in the previous section are different. The corresponding relationship and the *Z*-axis projection image are shown in Figs. 4(a) and 4(b), respectively.

Due to the different positions of (x_v, y_v), different angles α, β can be calculated according to the geometry and four regions, where $\delta_{\text{Top}} = 0$ and $\delta_{\text{Bottom}} = \pi$.

$$\alpha = \begin{cases} \arctan \frac{R - y_v}{R - x_v} + \frac{\pi}{2} + \delta & x_v \leqslant R; y_v \leqslant R \\ \arctan \frac{R - x_v}{y_v - R} + \delta & x_v \leqslant R; y_v > R \\ \arctan \frac{x_v - R}{R - y_v} + \pi - \delta & x_v > R; y_v \leqslant R \\ \arctan \frac{y_v - R}{x_v - R} + \frac{3\pi}{2} - \delta & x_v > R; y_v > R \end{cases} \tag{9}$$

$$\beta = \arctan \frac{\sqrt{\left(x_v - R\right)^2 + \left(y_v - R\right)^2}}{R} \tag{10}$$

Then, $\left(x_{p_{Top}}, y_{p_{Top}}\right)$ and $\left(x_{p_{Bottom}}, y_{p_{Bottom}}\right)$ of the top and bottom points are calculated as follows:

$$x_{p_{Top}}=\begin{cases}0 & \alpha>2\pi\\ \left(1-\dfrac{\alpha}{2\pi}\right)\times R_p & 0\leqslant\alpha\leqslant 2\pi\\ R_p\text{-}1 & \alpha<0\end{cases}\quad y_{p_{Top}}=\begin{cases}0 & \alpha<0\\ \dfrac{\alpha}{\pi}\times R_p & 0\leqslant\alpha\leqslant\pi\\ R_p\text{-}1 & \alpha>\pi\end{cases} \tag{11}$$

$$x_{p_{Bottom}}=\begin{cases}0 & \alpha<0\\ \dfrac{\alpha}{2\pi}\times R_p & 0\leqslant\alpha<2\pi\\ R_p\text{-}1 & \alpha\geqslant 2\pi\end{cases}\quad y_{p_{Bottom}}=\begin{cases}0 & \alpha>\pi\\ \left(1-\dfrac{\alpha}{\pi}\right)\times R_p & 0\leqslant\alpha\leqslant\pi\\ R_p\text{-}1 & \alpha<0\end{cases} \tag{12}$$

$$V_{(R_v-1-y_v,R_v-1-x_v)}=F\left(x_{p_{Top}},y_{p_{Top}}\right) \tag{13}$$

$$V_{(R_v-1-x_v,y_v)}=F\left(x_{p_{Bottom}},y_{p_{Bottom}}\right) \tag{14}$$

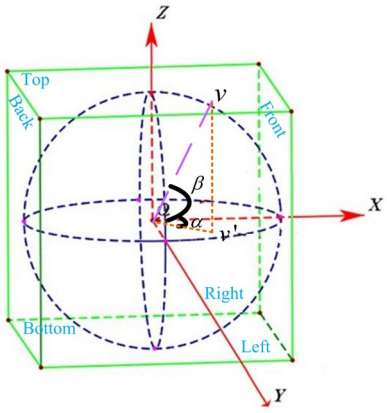

(a) The stereoscopic image

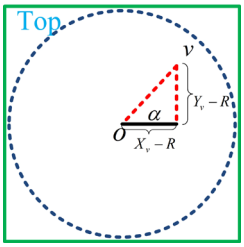

(b) The image from *Z*-axis direction projection

Figure 4: The image form vertical angle

2.4 Image reconstruction

The serration is appeared in the coordinate transformation process. Since the coordinates are rounded during the calculation, only a limited number of pixels are used. The spatial positions of the pixels are not considered. Thus, we follow the spatial position of the coordinates, and calculate the length of the four field weight of the coordinates with the Euclidean distance. The closer the distance, the greater the weight. As shown in Fig. 5, $\lfloor\bullet\rfloor$ is rounded down.

$$L_i=\langle P,A_i\rangle+0.01\qquad i=1,2,3,4 \tag{15}$$

$$w_i=\frac{1}{L_i}\qquad i=1,2,3,4 \tag{16}$$

where L_i is the coordinates of the distance, $\langle P, A_i \rangle$ is the Euclidean distance from point P to point A_i.

$$F(P) = \frac{\sum_{i=1}^{4} f(A_i) w_i}{\sum_{i=1}^{4} w_i} \tag{17}$$

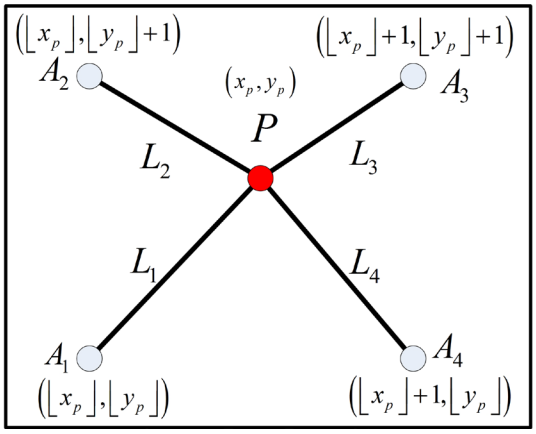

Figure 5: Weight distribution image

3 Experimental demonstrations

We choose 30 different shooting scenes for the experiment (indoor and field, etc). The horizontal of view is 360°, and the vertical field of view is 340°. The image resolution is 1024×1024.

3.1 Verify the effective of image reconstruction algorithm

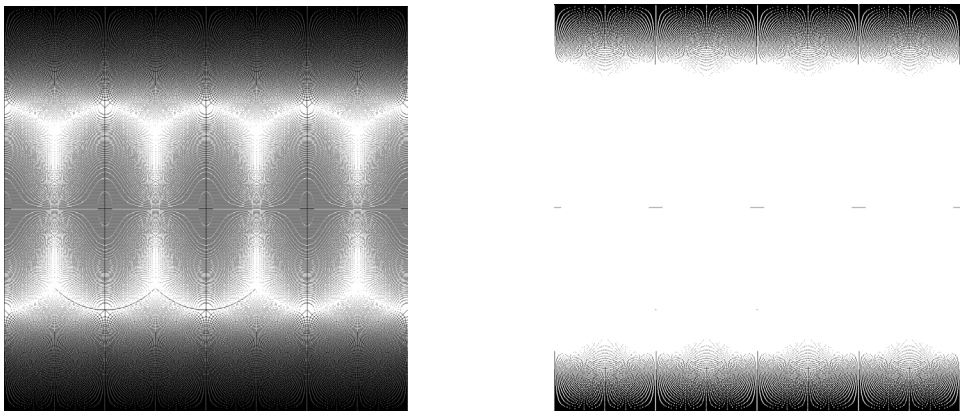

(a) Rounding mapping algorithm (b) Reconstruction mapping algorithm

Figure 6: Image of pixels

Figs. 6(a) and 6(b) are the pixel distribution of coordinate rounding mapping and the coordinate reconstruction algorithm, where white is the used pixel and black is the unused pixel. The pixel utilization rate of the coordinate rounding algorithm is 51%, while 84% is the pixel utilization rate of the coordinate reconstruction mapping algorithm with space position number of pixels is considered.

In Fig. 7, we can see that the coordinate direct mapping algorithm is rough on the edge as shown in Fig. 7(a), and the coordinate reconstruction algorithm with the information of pixel distance is considered to guarantee the clarity of the pixel and smooth the edge of the role.

(a) Direct mapping algorithm (b) Reconstruction mapping algorithm

Figure 7: Coordinate mapping algorithm

3.2 Show the result

The image multi-directional reconstruction effect of a car is shown in Figs. 8, 9 and 10 including a small space, indoor large space and outdoor large space. As shown in Fig. 8(e), the image of the roof skylight is restored, which is difficult to be available on the original. As shown in Fig. 9, they are the floor tiles and skylight images. The proposed algorithm considers the distance information of the coordinate map and reduces the linear characteristics of the floor brick lines. As shown in Fig. 10(f), the distortion is produced in the vertical angle between 320° and 340°, because the camera shoots from the ground and also in the strong light. Therefore, it needs further study.

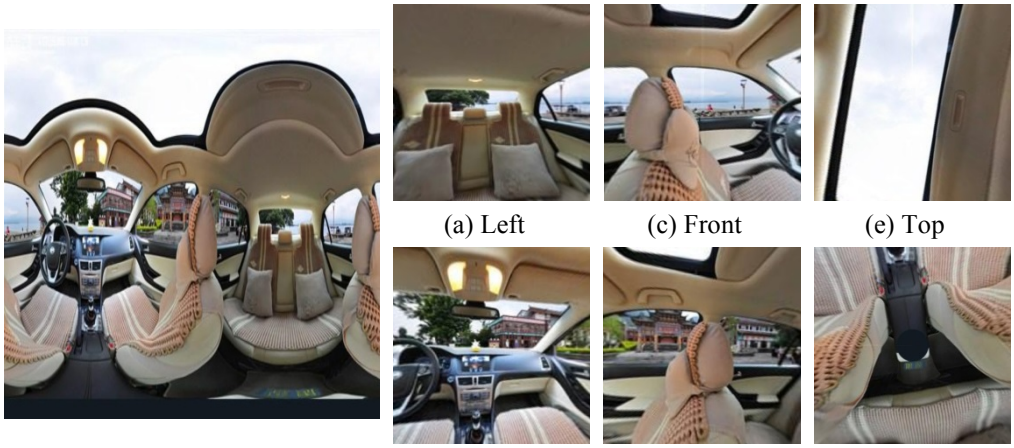

(a) The Panoramic image (a) Left (c) Front (e) Top (b) Right (d) Back (f) Bottom

Figure 8: Multi-directional reconstruction effect of inside car image

(a) The Panoramic image (a) Left (b) Right (c) Front (d) Back (e) Top (f) Bottom

Figure 9: Multi-directional reconstruction effect of interior image

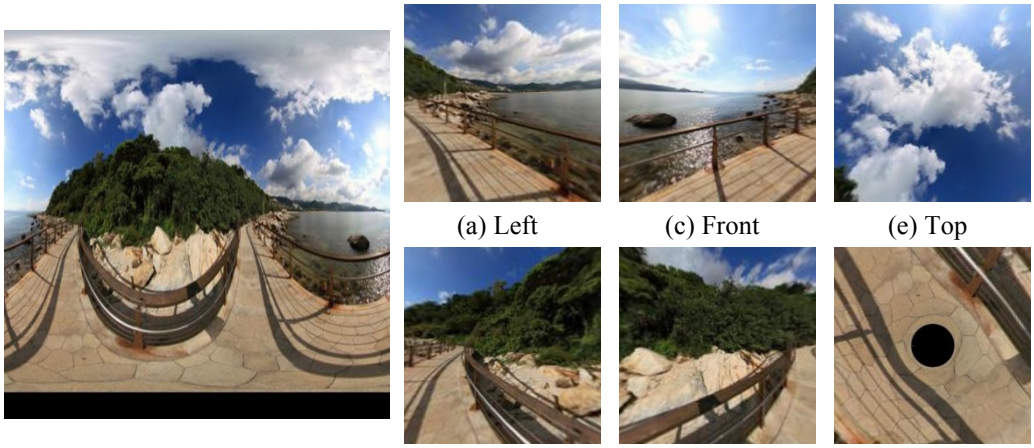

(a) The Panoramic image (a) Left (b) Right (c) Front (d) Back (e) Top (f) Bottom

Figure 10: Multi-directional reconstruction effect of outdoor image

4 Conclusion

In order to solve the distortion of panoramic images, a multi-azimuth reconstruction algorithm is proposed for the panoramic camera. Considering the coordinate mapping transformation and the coordinate space position information, the distance weight model is built, and the multi-azimuth image reconstruction is realized. Good results are achieved. However, when the outdoor lights are strong, the non-linear distortion requires further study.

Funding Statement: This work is supported by Light of West China (Grant No. XAB2016B23), Chinese Academy of Sciences. And the Open Project Program of the State Key Lab of CAD & CG (Grant No. A2026), Zhejiang University.

Conflicts of Interest: The authors declare that they have no conflicts of interest to report regarding the present study.

References

Alomran, M.; Chai, D. (2016): Feature-based panoramic image stitching. *14th International Conference on Control, Automation, Robotics and Vision*, pp. 1-6.

Cai, C.; Wang, P.; Liang, Y. H. (2016): Fast image stitching based on improved SURF. *IEEE 20th International Conference on Computer Supported Cooperative Work in Design*, pp. 411-416.

Cheng, K.; Hui, K.; Zhan, Y.; Li, M. (2017): Sparse representations based distributed attribute learning for person re-identification. *Multimedia Tools and Applications*, vol. 76, no. 23, pp. 25015-25037.

Cheng, K.; Xu, F.; Tao, F.; Qi, M.; Li, M. (2018): Data-driven pedestrian re-identification based on hierarchical semantic representation. *Concurrency and Computation: Practice and Experience*, vol. 30, no. 23, e4403.

Lee, J.; Kim, B.; Kim, K.; Kim, Y.; Noh, J. (2016): Rich360: optimized spherical representation from structured panoramic camera arrays. *ACM Transactions on Graphics*, vol. 35, no. 4, pp. 63.

Liu, S.; Zhao, L.; Li, J.; Cai, Q. (2014): The SIFT features matching for spherical panoramic images. *In 11th IEEE International Conference on Control & Automation*, pp. 914-917.

Ma, X.; Liu, D.; Zhang, J.; Xin, J. (2015): A fast affine-invariant features for image stitching under large viewpoint changes. *Neurocomputing*, vol. 151, pp. 1430-1438.

Mühlhausen, M.; Magnor, M. (2020): Multiview panorama alignment and optical flow refinement. *Real VR-Immersive Digital Reality*, pp. 96-108.

Pan, L.; Qin, J.; Chen, H.; Xiang, X.; Li, C. et al. (2019): Image augmentation-based food recognition with convolutional neural networks. *Computers*, *Materials & Continua*, vol. 59, no. 1, pp. 297-313.

Pham, N. T.; Lee, J. W.; Kwon, G. R.; Park, C. S. (2019): Efficient image splicing detection algorithm based on Markov features. *Multimedia Tools and Applications*, vol. 78, no. 9, pp. 12405-12419.

Qiu, S.; Luo, J.; Yang, S.; Zhang, M.; Zhang, W. (2019): A moving target extraction algorithm based on the fusion of infrared and visible images. *Infrared Physics & Technology*, vol. 98, pp. 285-291.

Sacht, L.; Velho, L. (2013): Complex plane transformations for manipulation and visualization of panoramas. *GRAPP/IVAPP*, pp. 179-184.

Sandnes, F. E.; Huang, Y. P. (2016): Translating the viewing position in single equirectangular panoramic images. *IEEE International Conference on Systems, Man, and Cybernetics*, pp. 389-394.

Shaikh, T. S.; Patankar, A. B. (2015): Multiple feature extraction techniques in image stitching. *International Journal of Computer Applications*, vol. 123, no. 15.

Sharpless, T. K.; Postle, B.; German, D. M. (2010): Pannini: a new projection for rendering wide angle perspective images. *Proceedings of the Sixth International Conference on Computational Aesthetics in Graphics, Visualization and Imaging, Eurographics Association*, pp. 9-16.

Shi, H.; Lei, X.; Wan, F. (2019): Spatial calibration method for master-slave camera based on panoramic image mosaic. *Optical Engineering*, vol. 58, no. 4, 043105.

Tehrani, M. H.; Garratt, M. A.; Anavatti, S. G. (2016): Low-altitude horizon-based aircraft attitude estimation using UV-filtered panoramic images and optic flow. *IEEE Transactions on Aerospace and Electronic Systems*, vol. 52, no. 5, pp. 2362-2375.

Wei, J.; Li, C. F.; Hu, S. M.; Martin, R. R.; Tai, C. L. (2011): Fisheye video correction. *IEEE Transactions on Visualization and Computer Graphics*, vol. 18, no. 10, pp. 1771-1783.

Yuan, C. H.; Pan, J. S.; Sheu, M. H.; Chen, T. H. (2013): Fast image blending and deghosting for panoramic video. *Ninth International Conference on Intelligent Information Hiding and Multimedia Signal Processing*, pp. 104-107.

Zeng, L.; Zhang, S.; Zhang, J.; Zhang, Y. (2014): Dynamic image mosaic via SIFT and dynamic programming. *Machine Vision and Applications*, vol. 25, no. 5, pp. 1271-1282.

Zhang, D.; Liang, Z.; Yang, G.; Li, Q.; Li, L. et al. (2018): A robust forgery detection algorithm for object removal by exemplar-based image inpainting. *Multimedia Tools and Applications*, vol. 77, no. 10, pp. 11823-11842.

Zhang, D.; Yin, T.; Yang, G.; Xia, M.; Li, L. et al. (2017): Detecting image seam carving with low scaling ratio using multi-scale spatial and spectral entropies. *Journal of Visual Communication and Image Representation*, vol. 48, pp. 281-291.

Zhu, L.; Liu, Y.; Lai, S.; Li, J. (2016): Expanding a fish-eye panoramic image through perspective transformation. *3rd International Conference on Systems and Informatics*, pp. 871-875.